

# Prediction with Spatio-temporal Point Processes with Self Organizing Decision Trees

Oğuzhan Karaahmetoğlu and Suleyman S. Kozat *Senior Member, IEEE*

**Abstract**—We study the spatio-temporal prediction problem, which has attracted attention of many researchers due to its critical real-life applications. In particular, we introduce a novel approach to this problem. Our approach is based on the Hawkes process, which is a non-stationary and self-exciting point process. We extend the formulations of a standard point process model that can represent time-series data to represent a spatio-temporal data. We model the data as nonstationary in time and space. Furthermore, we partition the spatial region we are working on into subregions via an adaptive decision tree and model the source statistics in each subregion with individual but mutually interacting point processes. We also provide a gradient based joint optimization algorithm for the point process and decision tree parameters. Thus, we introduce a model that can jointly infer the source statistics and an adaptive partitioning of the spatial region. Finally, we provide experimental results on a real-life data, which provides significant improvement due to space adaptation and joint optimization compared to standard well-known methods in the literature.

**Index Terms**—Spatio-temporal prediction, point process, Hawkes process, decision tree, online learning, nonstationary time-series data, earthquake prediction.

**EDICS Category: MLR-APPL, MLR-LEAR**

## I. INTRODUCTION

### A. Preliminaries

Every moment, from thousands of human activities and millions of sensor readings, new instances of data in various structures and types are generated and collected. Among these types, spatio-temporal data collection has been an essential part of developing solutions to many real-life problems such as spatio-temporal prediction, dynamic-system modeling and data assimilation. Spatio-temporal data refers to a collection of samples that are indexed by time and distributed along a two dimensional spatial region. Spatio-temporal prediction is estimating the time and the location of a sample using only the information about the past. This problem carries vital importance as it covers many real-life problems such as earthquake prediction [1], [2], crime prediction and social action prediction [3], [4]. Early prediction of the time and location of earthquakes and criminal events could save many

lives whereas predicting malfunctions in an industrial facility could reduce maintenance costs [5].

Due to these critical applications, many solutions have been proposed such as deep architectures [6], [7]. Among them the Recurrent Neural Networks (RNN) [8] seem to be the dominant approach [9], [10]. This is due to the inherent memory of the RNNs, which allows them to carry past information over time. Different variations of RNNs were applied to the same problem for comparison. Thanks to their internal gated structure, Long Short Term Memory (LSTM) [11] networks were shown to be superior. Other than the RNN and its variants, Convolutional Neural Networks (CNN) [12] were also used in spatio-temporal prediction problem as they can learn the interaction between different spatial locations [6], [13]. Despite their abilities, deep architectures are not directly applicable to real-life data, which are sparse and non-stationary to train deep architectures [14], [6].

To overcome the problems due to the nonstationarity and the sparsity of the data, researchers also use point processes and statistical models for prediction [7], [15]. This approach aims to represent the samples in the spatio-temporal data directly. Point processes have been used to model various real-life time-series data [16], [17]. There are also previous works that introduce spatio-temporal point process mechanisms that can model the time indexes and locations of the samples together [16], [17].

In this paper, we introduce a novel approach for the spatio-temporal prediction problem. Our approach is based on point processes as we work on nonstationary and highly sparse data. We extend the formulations of a point process model and apply it to spatio-temporal data. We model the sample observations as a space-varying process. Therefore, we partition the spatial region into subregions and model the sample observation mechanisms in each subregion with individual but mutually interacting point processes. We use a decision tree to partition the spatial region. Point process we use to model the sample observations in each subregion is the Hawkes process [18]. Thanks to the self-exciting property of Hawkes processes and the spatial partitioning mechanism, we can apply our model effectively to real-life problems such as earthquake prediction or crime prediction where the data is sparse and nonstationary in time and space. Furthermore, we jointly optimize the spatial partitions and the point process parameters in each partition. Moreover, our solution is suitable for online setup as we optimize our model parameters with stochastic gradient based updates.

This work is supported in part by Outstanding Researcher Programme Turkish Academy of Sciences.

S. S. Kozat and O. Karaahmetoğlu are with the Department of Electrical and Electronics Engineering, Bilkent University, Bilkent, Ankara 06800, Turkey, Tel: +90 (312) 290-2336, Fax: +90 (312) 290-1223, (contact e-mail: {kozat, koguzhan}@ee.bilkent.edu.tr).

S. S. Kozat and O. Karaahmetoğlu are also with the Data-Boss A.S., Bilkent Cyberpark, Ankara 06800, (email: {serdar.kozat, oguzhan.karaahmetoglu}@data-boss.com.tr)

## B. Prior Art and Comparisons

Deep neural networks have been successfully used in many areas [19], [20]. Due to their complex structures, they can model highly non-linear and complex patterns [8], [12]. Thanks to their inherent memory, some variants of deep models such as RNNs and LSTMs can capture the temporal dependencies on time-series data [11]. Despite their ability to model complex patterns in time series data, deep models are error-prone under nonstationary and sparse data, which is the general case in spatio-temporal data [6], [21]. Moreover, deep architectures generally accept structured data, which is also not the case in our data as the time indexes of samples can be unevenly spaced and the spatial locations of the samples can be at any arbitrary location. To overcome these problems, unstructured data is generally converted into a structured form by binning the samples into fixed size spatio-temporal intervals [6], [21]. However, this approach could change the problem description as it no longer assumes continuous time indexes and continuous spatial distribution. Moreover, model estimations for sample observation times and locations are for the discrete spatio-temporal bins. In our approach, we do not discretize the input data into fixed size spatio-temporal intervals. Thus, we directly work on the continuous data without applying any adhoc preprocessing step that changes the continuous structure of the data.

Point processes are also used in spatio-temporal prediction problem [17]. A standard point process model such as Hawkes or Poisson can model time-series data [16], [18]. There are also previous works that apply such probabilistic models to spatio-temporal data with certain modifications. These modifications extend the formulation of the temporal point process to model spatial locations as well [16] or to independently estimate spatial locations as in the marked point processes [17]. Finally, point process approaches are generally not applicable to online setups as they generally require the whole dataset for parameter optimization [22]. On the other hand, our model is applicable to online setup as it can be updated with new sample observations. Furthermore, we adaptively partition the spatial space adaptively using decision trees. Therefore, the model captures the time-varying and space-varying characteristics jointly.

In this paper, we introduce an objective function and we use it to jointly optimize our model parameters. Our objective function is based on the likelihood of the probabilistic model that we fit on the spatio-temporal data. This approach is used in previous works as well, however, we modify the standard likelihood function so that we can control the behavior of the parameter optimization procedure. Unlike the most of the approaches based on the point process modeling such as [22] and [16], we update our model parameters based on gradients of the objective function with respect to model parameters.

## C. Contributions

Our main contributions are:

- 1) As the first time in the literature, we introduce a novel architecture that can adaptively partition a spatial region into subregions and infer the interaction between these

regions simultaneously. Therefore, we jointly optimize the model parameters with gradient-based updates.

- 2) We introduce a spatio-temporal prediction model based on point processes where we maximize the likelihood of a probabilistic model with gradient based parameter optimization. Thus, we efficiently train our algorithm to capture the patterns in sparse data in an online manner.
- 3) We present an extended formulation of the Hawkes process with adaptive spatial partitioning based on self-organizing decision trees. Hence, our formulation for the extended Hawkes process covers the space-varying sample observation mechanism in spatio-temporal data.
- 4) Through extensive set of experiments, we show that our models can represent the spatio-temporal samples in real life data such as earthquake data, which is highly nonstationary. We also demonstrate significant performance improvements with respect to standard well-known methods.

## D. Organization of the Paper

In the following section, we introduce our problem description. In section III-A, we give a brief information about the probabilistic model we use. In section III-B, we describe the spatial partitioning and the spatial kernel mechanism we use to extend the probabilistic model. In sections III-C and III-D, we explain the procedure for estimating the times and locations of spatio-temporal samples and the procedures for optimizing our model parameters. In section IV, we give experimental results on both simulation data and real-life data. Finally, in section V, we give the concluding remarks.

## II. MODEL AND PROBLEM DESCRIPTION

We denote the vectors with boldface lowercase letters, e.g.  $\mathbf{x} = [x^{(0)}, x^{(1)}, \dots, x^{(L)}]$  is a vector with length  $L$ . We denote the matrices with boldface uppercase letters, e.g.  $\mathbf{X}$ . The notation  $\mathbf{X}_{i,j}$  refers to the element of the matrix at the  $i$ th row and the  $j$ th column. The notation  $\mathbf{X}_{i,:}$  is the  $i$ th row of the matrix  $\mathbf{X}$  and  $\mathbf{X}_{:,j}$  is the  $j$ th column of the matrix  $\mathbf{X}$ . The notation  $\mathbf{x}^T$  refers to the ordinary transpose of a vector and  $\|\mathbf{x}\|^2 = \langle \mathbf{x}, \mathbf{x} \rangle = \mathbf{x}^T \mathbf{x}$  is the  $\ell^2$  norm of a vector.  $\odot$  operator is the element-wise multiplication and  $\mathbb{1}_L$  is a column vector of ones with length  $L$ . Unless otherwise stated, all vectors in this paper are column vectors and real vectors.

In spatio-temporal data, samples are distributed along three axes, two spatial axes and a temporal axis. Such a distribution is visualized in Fig. 1. Spatial positions  $\mathbf{s} = (m, n)$ , which are shown as  $\{\mathbf{s}_i\}_{i=1}^4$  in Fig. 1 as an example, are tuples describing the geological positioning, e.g. latitude and longitude. Temporal positions  $t$ , which are shown as  $\{t_i\}_{i=1}^4$  in Fig. 1 as an example, are timestamps, e.g. times of events. We work on continuous data, hence  $t_i \in \mathbb{R}$  and  $m, n \in \mathbb{R}$ . Together, these three axes provide all the information about a sample in a spatio-temporal dataset. Thus, we are given a set of samples  $X = \{\mathbf{x}_i\}_{i=1}^I$ , where each sample  $\mathbf{x}_i = [t_i, \mathbf{s}_i] = [t_i, (m_i, n_i)]$  is represented by a timestamp  $t_i$ , which we refer to as the observation time and a geological stamp  $\mathbf{s}_i$ , which we refer to as the spatial location as shown in Fig. 1.

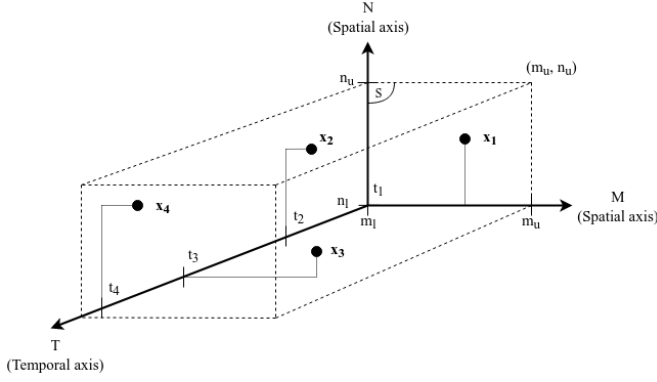


**Fig. 1:** Spatio-temporal data distribution. Samples  $\mathbf{x}_1$ ,  $\mathbf{x}_2$ ,  $\mathbf{x}_3$  and  $\mathbf{x}_4$  are spatio-temporal samples that are distributed along a temporal axis,  $T$ , and two spatial axes,  $M$  and  $N$ . Also note that the spatial region that we work on is bounded in a spatial region  $S$ , which has the lower bounds  $(m_l, n_l)$  and upper bounds  $(m_u, n_u)$  in spatial axes.

We define the set of observation times as  $\{t_i\}_{i=1}^I$ . We also define the function "history" at time  $t$  as  $H(t) = \{\mathbf{x}_i | t_i < t\}_{i=1}^I$ , i.e. all the past samples until the time  $t$ . The aim is to predict the next observation time  $t_i$  and the spatial location  $\mathbf{s}_i$  of a sample,  $\mathbf{x}_i = [t_i, \mathbf{s}_i]$  given the history  $H(t_i)$ . Hence, we introduce a function  $F$ , which estimates the observation time and the spatial location of a sample  $\mathbf{x}_i$  as

$$\hat{\mathbf{x}}_i = [\hat{t}_i, \hat{\mathbf{s}}_i] = F(H(t)),$$

where  $\hat{\mathbf{x}}_i = [\hat{t}_i, \hat{\mathbf{s}}_i]$  is the estimated observation time and spatial location of the sample  $\mathbf{x}_i$ . We evaluate the performance of our estimation  $\hat{\mathbf{x}}_i$  for a sample  $\mathbf{x}_i$  with a loss function

$$l(\hat{\mathbf{x}}_i, \mathbf{x}_i) = [(\hat{t}_i - t_i)^2, (\hat{m}_i - m_i)^2, (\hat{n}_i - n_i)^2]. \quad (1)$$

**Remark 1.** We use the squared error to report experimental results. However, we can also use any  $\ell^p$  loss function,

$$l(\hat{\mathbf{x}}_i, \mathbf{x}_i) = [|\hat{t}_i - t_i|^p, |\hat{m}_i - m_i|^p, |\hat{n}_i - n_i|^p].$$

For multiple samples, we evaluate the performance with the loss  $L(\hat{X}, X)$ , where the sets  $\hat{X}$  and  $X$  are the paired estimation and the ground-truth samples.  $L$  is defined as

$$L(\hat{X}, X) = \frac{1}{I} \sum_{i=1}^I l(\hat{\mathbf{x}}_i, \mathbf{x}_i). \quad (2)$$

Here, the function  $F$  is the expectation of the observation time and spatial location  $(\hat{t}_i, \hat{\mathbf{s}}_i) = \mathbb{E}[\hat{t}_i, \hat{\mathbf{s}}_i | H(t_{i-1})]$ , where  $\hat{t}_i$  and  $\hat{\mathbf{s}}_i$  are random variables with probability density functions  $f_{\hat{t}_i}$  and  $f_{\hat{\mathbf{s}}_i}$ . Random variables  $\hat{t}_i$  and  $\hat{\mathbf{s}}_i$  are the observation time and spatial location of the sample  $\mathbf{x}_i$ . We model the probability density functions with a point process. Therefore, in the next subsection we give a brief information about the point process models.

#### A. Representation of Sample Observations with Point Processes

Point processes model the likelihood of observing a sample at time  $t$  given the history  $H(t)$ . Probability density function for spatio-temporal samples is defined as

$$f_{\hat{t}_i}(t|H(t)) = \lim_{\Delta t \rightarrow 0} \Pr(N(t) - N(t - \Delta t) = 1 | H(t)), \quad (3)$$

where  $N(t)$  is the total number of sample observations up to time  $t$  [18]. A point process, and the density function defined in (3), is characterized by its conditional intensity function  $\lambda(t|H(t))$  [18].  $\lambda(t|H(t))$  is given as

$$\lambda(t|H(t)) = \lim_{\Delta t \rightarrow 0} \frac{\Pr(N(t + \Delta t) - N(t) = 1 | H(t))}{\Delta t}, \quad (4)$$

which is the expected number of sample observations in an infinitesimal time interval around  $t$ . The density function in (3) can be expressed in terms of the conditional intensity function if it is approximated by Bernoulli trials with  $\Delta t \rightarrow 0$  as

$$f_{\hat{t}_i}(t|H(t)) = \lambda(t|H(t)) e^{-\int_{t_{i-1}}^t \lambda(t'|H(t')) dt'}, \quad (5)$$

where  $t_{i-1}$  is the observation time of the last event before the time  $t_i$ .

The intensity  $\lambda(t|H(t))$  controls the frequency of the sample observations, i.e. the higher the intensity the more frequently samples will be observed. In certain point processes, such as Poisson, this intensity is constant, i.e.  $\lambda(t) = \lambda$ . Thus, the process is stationary in time [18]. However, a more general formulation of the conditional intensity is presented in Hawkes processes in which the intensity is a function of previous sample observation times as

$$\lambda(t|H(t)) = \mu + \sum_{t_j < t} e^{-\gamma(t-t_j)}, \quad (6)$$

where  $\{t_j\}_j$  are the observation times of the samples before  $t$ ,  $\mu$  is called the background intensity and  $\gamma$  is called the decay rate.

The intensity formulation in (6) yields a nonstationary process due to the time-varying temporal kernel  $g(t-t_j) = e^{-\gamma(t-t_j)}$  for every past sample. Hence, Hawkes processes can represent various real-life time-series data [16], [21]. Nevertheless, this intensity function lacks the spatial location information of samples and the interaction among the spatial locations of the past samples. Since our aim is to estimate the sample observation times and spatial locations via inferring the representation of the samples, we introduce a modification for the conditional intensity in (6) to add spatial interactions with a spatial kernel. We describe this spatial kernel in detail in the following section.

### III. A NOVEL SPATIO-TEMPORAL POINT PROCESS MODEL

Here, we describe the adaptive tree structure to partition the spatial region into fixed number of adaptive subregions. We first describe how an adaptive decision tree works and explain how we select and optimize a point process to model the sample observation times in each subregion. Moreover, we introduce our objective function as well as the training procedure of our model.

#### A. A Conditional Intensity Function with Spatial and Temporal Kernels

In this section, we present the spatial kernel that we introduce as an extension to the conditional intensity function in (6). We introduce a spatial kernel based on decision trees that adaptively partition the spatial space into subregions based on the observation in an online manner.

Suppose that the set of samples  $X = \{\mathbf{x}_i\}_{i=1}^I$  are distributed in a bounded spatial region  $S = [[m_l, m_u], [n_l, n_u]]$  as shown in Fig. 1, i.e.  $m_i \in [m_l, m_u]$ ,  $n_i \in [n_l, n_u] \forall \mathbf{x}_i$  where  $m_l$  and  $n_l$  are the lower bounds of the two spatial axes and  $m_u$  and  $n_u$  are the upper bounds as shown in Fig. 1.

Recall that the intensity function of the Hawkes process is time-varying. Therefore, the intensity is changing over time depending on the past sample times. In spatio-temporal prediction problem, the intensity could be space-varying as well to model non-stationary real life data. Thus, we extend the definition of the intensity in (4) to be the expected number of sample observations in an infinitesimal spatio-temporal interval around the time  $t$  and the location  $\mathbf{s}$ , i.e.

$$\lambda(t, \mathbf{s}|H(t)) = \lim_{\Delta t \rightarrow 0, \Delta s \rightarrow 0} \frac{Pr(N(t + \Delta t, \bar{\mathbf{s}}) - N(t) = 1|H(t))}{\Delta t \Delta s} \quad (7)$$

where the term  $\bar{\mathbf{s}}$  is the spatial region around the location  $\mathbf{s}$  with radius  $\Delta s$ , i.e.  $\bar{\mathbf{s}} = \{(m, n) \in \mathbb{R}^2 \mid \|\mathbf{s} - (m, n)\|^2 \leq \Delta s\}$ . Consequently, the function  $N(t)$  can be extended as  $N(t, \bar{\mathbf{s}})$ , the number of events up to time  $t$  and the number of events around the spatial location  $\mathbf{s}$  at time  $t$ .

We require a formulation for a time-varying and space-varying conditional intensity function. To this end, we partition the space  $S$  into fixed number of adaptive subregions,  $\{S_k\}_{k=1}^K$ , such that  $\bigcup_{k=1}^K S_k = S$  and  $S_i \cap S_j = \emptyset$ . We define the set  $X_k$  as the collection of samples that belong to the subregion  $S_k$ , i.e.  $X_k = \{\mathbf{x}_j | \mathbf{s}_j \in S_k\}_{j=1}^N$  such that  $X = \bigcap_{k=1}^K X_k$  and  $X_i \cap X_j = \emptyset$ .

We also define a vector  $\mathbf{p}(\mathbf{s}) = [p_k(\mathbf{s})]_{k=1}^K$  for any spatial location  $\mathbf{s}$  as the subregion vector where

$$p_k(\mathbf{s}) = \begin{cases} 1, & \text{if } \mathbf{s} \in S_k \\ 0, & \text{otherwise.} \end{cases} \quad (8)$$

The vector  $\mathbf{p}(\mathbf{s})$  is a one-hot vector indicating the subregion in which the location  $\mathbf{s}$  falls. We represent the sample observation mechanism in each subregion with an intensity function. Hence, for a subregion  $S_k$ , the conditional intensity is  $\lambda_k(t, H(t))$ . For any point in spatio-temporal space, we compute the conditional intensity  $\lambda(t, \mathbf{s}|H(t))$  as the conditional intensity of the subregion where the location  $\mathbf{s}$  falls. It is given as,

$$\lambda(t, \mathbf{s}|H(t)) = \mathbf{p}(\mathbf{s})^T \boldsymbol{\lambda}(t, \mathbf{s}|H(t)), \quad (9)$$

where  $\boldsymbol{\lambda}(t, \mathbf{s}|H(t)) = [\lambda_k(t, \mathbf{s}|H(t))]_{k=1}^K$ . Alternatively, we formulate the spatio-temporal conditional intensity as

$$\lambda(t, \mathbf{s}|H(t)) = \begin{cases} \lambda_1(t|H(t)), & \text{if } \mathbf{s} \in S_1 \\ \lambda_2(t|H(t)), & \text{if } \mathbf{s} \in S_2 \\ \dots & \\ \lambda_K(t|H(t)), & \text{if } \mathbf{s} \in S_K. \end{cases} \quad (10)$$

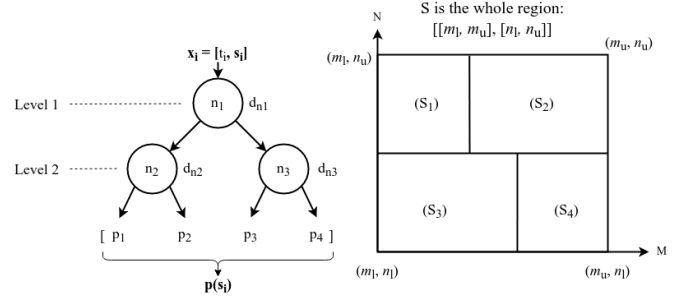


**Fig. 2:** Diagram of a 2-level decision tree. The decision tree has the nodes  $n_1, n_2, n_3$ , which have the decision functions  $d_{n_1}, d_{n_2}, d_{n_3}$ . For the input sample  $\mathbf{x}_i$ , the subregion scores are  $\mathbf{p}(\mathbf{s}_i)$  for 4 branch leaves. These 4 branches correspond to the 4 subregions, which are shown as  $S_1, S_2, S_3$  and  $S_4$ .

We also add a spatial kernel to the intensity  $\lambda_k(t|H(t))$  as

$$\lambda_k(t|H(t)) = \mu_k + \sum_{t_j < t} g_k(t - t_j) h_k(\mathbf{s}_j). \quad (11)$$

We use the same temporal kernel as in (6) and choose the spatial kernel  $h_k(\mathbf{s}_j)$  in (11) as

$$h_k(\mathbf{s}_j) = \boldsymbol{\Gamma}_{:,k}^T \mathbf{p}(\mathbf{s}_j), \quad (12)$$

where  $\boldsymbol{\Gamma}$  is the  $K \times K$  interaction matrix. The element  $\boldsymbol{\Gamma}_{i,j}$  of the interaction matrix represents the effect of a sample  $x \in X_i$  to the intensity of the subregion  $S_j$ . The vector  $\mathbf{p}(\mathbf{s}_j)$  is the subregion vector with elements  $p_k(\mathbf{s}_j)$  as defined in (8).

We limit the effect of the past samples to the current intensity by truncating the summation in (11), which accumulates the past event effects. We only accumulate the last  $\phi$  samples so that the scale of the sum stays constant over the whole sequence. Furthermore, we define the set  $X_H(t)$  as the most recent  $\phi$  samples before the time  $t$ .

We partition the spatial region  $S$  with adaptive decision trees where the subregions are adaptively organized to represent the partitions in time. Therefore, as the source statistics generating the samples change, partitioning of the spatial region could change as well. In the next subsection, we explain the adaptive tree structure we use in detail.

## B. Spatial Partitioning with Adaptive Decision Trees

The decision tree structure that we use is a hierarchical collection of nodes,  $D = \{n_r\}_{r=1}^R$ . As shown in Fig. 2, each node has two branches connecting to two child nodes except the leaf nodes, which are located at the bottom of the tree (at level  $L = 2$ ). The node  $n_1$ , in Fig. 2 is called the root node.

**Remark 2.** Note that we use a 2-level decision tree for presentation simplicity. Our formulation covers different depths as well.

Starting from the root node  $n_1$ , we assign a sample  $\mathbf{x}_i$  to the left or right child of the current node until we reach the leaf nodes. Therefore, each node  $n_r$  is associated with a binary decision  $d_{n_r}(\mathbf{x}_i)$ , where  $d_{n_r}$  is a function with range  $\{-1, +1\}$ . In previous works [23], [24], the decision  $d_{n_r}(\mathbf{x}_i)$  is based on a randomly selected feature  $x_i^{(f_{n_r})}$  of the sample  $\mathbf{x}_i$  with features  $\mathbf{x}_i = [x_i^{(f)}]_{f=1}^F$  as

$$d_{n_r}(\mathbf{x}_i) = \text{sign}(x_i^{(f_{n_r})} - b_{n_r}) \leq 0, \quad (13)$$

where  $x_i^{(f_{n_r})}$  is the feature selected at the node  $n_r$  for decision and  $b_{n_r}$  is the threshold value for comparison. If (13) is positive, the sample  $\mathbf{x}_i$  will be assigned to the left node and to the right node otherwise.

With the decisions made at every node with a decision function as in (13), we separate the samples according to their spatial locations by comparing them using the threshold  $b_{n_r}$ . The feature space is the spatial space  $S$ , which is shown in Fig. 2. Therefore,  $x_i^{(f_{n_r})}$  can be either  $m_i$  or  $n_i$  for the sample  $\mathbf{x}_i$  at the spatial location  $\mathbf{s}_i = (m_i, n_i)$ . At every level of the decision tree, we split the spatial space  $S$  into smaller subregions and therefore assign samples into these groups. For a decision tree with  $L$  levels, we have  $K = 2^L$  leaf branches corresponding to the spatial subregions  $\{S_k\}_{k=1}^K$  as shown in Fig. 2 for  $K = 4$  case as an example.

We modify (13) by considering all the features  $[x_i^{(f)}]_{f=1}^F$ , i.e. both the  $m_i$  and  $n_i$  of the sample  $\mathbf{x}_i$ , in a single decision. Hence, our decisions have the form

$$d_{n_r}(\mathbf{x}_i) = \text{sign}(\mathbf{w}_{n_r}^T \mathbf{s}_i - b_{n_r}) \leq 0, \quad (14)$$

where  $\mathbf{w}_{n_r}$  is the vector of weights scaling the sample features  $\mathbf{s}_i$ .

Instead of dividing the feature space into partitions as in (8), we adapt the boundaries as follows. We replace the hard function in the decisions with the sigmoid function ( $\sigma(x) = 1/(1 + e^{-x})$ ) as

$$d_{n_r}(\mathbf{x}_i) = \sigma(\mathbf{w}_{n_r}^T \mathbf{x}_i - b_{n_r}), \quad (15)$$

which yields a value between  $[0, 1]$ . Soft functions in trees were previously used in [25] for source coding. For the binary decision functions that have the form in (14), a sample can only fall into a single subregion among  $\{S_k\}_{k=1}^K$ . Therefore, the subregion vector  $\mathbf{p}(\mathbf{s}_i)$  of a sample  $\mathbf{x}_i$  is a one-hot vector. However, we remove this hard separation by using a decision boundary that has the form in (15). With decision functions as in (15), instead of assigning a sample  $\mathbf{x}_i$  to either left or right branch, we compute the scores  $d_{n_r}(\mathbf{x}_i)$  and  $1 - d_{n_r}(\mathbf{x}_i)$  for left and right branches and assign the sample  $\mathbf{x}_i$  to both branches depending on the data, thereby introducing adaptiveness.

Instead of representing the spatial location  $\mathbf{s}_i$  of the sample,  $\mathbf{x}_i$ , with a one-hot subregion vector  $\mathbf{p}(\mathbf{s}_i)$ , we compute a vector of scores  $\mathbf{p}(\mathbf{s}_i) = [p_k(\mathbf{s}_i)]_{k=1}^K$ ,  $p_k(\mathbf{s}_i) \in [0, 1] \forall k$ . We name the vector of scores,  $\mathbf{p}(\mathbf{s}_i)$ , as the subregion scores. We compute the subregion scores  $\mathbf{p}(\mathbf{s}_i)$  by multiplying scores obtained at each branch starting from the root node until reaching to the leaf branches. We define the sequence of branches and sequence of visited nodes to reach the leaf  $k$  as  $\tau_k$  and  $\nu_k$ , e.g. for a depth-2 tree as shown in Fig. 2, second leaf branch  $p_2$  is reached if the left branch and then the right branch is taken at the first and the second levels. Thus,  $\tau_2 = [\text{left}, \text{right}]$  and  $\nu_2 = [n_1, n_2]$ . Therefore, we express the subregion score  $p_k(\mathbf{x}_i)$  for a leaf branch  $k$  as

$$p_k(\mathbf{x}_i) = \prod_{l=1}^L \pi(\mathbf{x}_i, \nu_k^{(l)}, \tau_k^{(l)}), \quad (16)$$

where  $\nu_k^{(l)}$  is the node visited and  $\tau_k^{(l)}$  is the direction of the branch taken at level  $l$  to reach the branch leaf  $k$ . The function  $\pi(\mathbf{x}_i, \nu_k^{(l)}, \tau_k^{(l)})$  is the score at level  $l$ , which is given as

$$\pi(\mathbf{x}_i, \nu_k^{(l)}, \tau_k^{(l)}) = \begin{cases} d_{\nu_k^{(l)}}(\mathbf{x}_i), & \text{if } \tau_k^{(l)} = \text{left} \\ 1 - d_{\nu_k^{(l)}}(\mathbf{x}_i), & \text{if } \tau_k^{(l)} = \text{right}. \end{cases} \quad (17)$$

**Remark 3.** The score vector we calculate satisfies the following properties:

- $\kappa = \arg \max_{k \in \{0, 1, \dots, K\}} [p_k(\mathbf{x}_i)] \Leftrightarrow \mathbf{s}_i \in S_\kappa$ , i.e. the maximum subregion score is obtained for the subregion in which the spatial location,  $\mathbf{s}_i$  of the sample  $\mathbf{x}_i$  falls.
- $\sum_{k=1}^K p_k(\mathbf{s}_i) = 1$ , i.e. sum of subregion scores are 1 for any location  $\mathbf{s}_i \in S$ .

Therefore, we compute a spatial subregion score  $\mathbf{p}(\mathbf{x}_i)$  with an adaptive decision tree and compute a vector of scores to be used in the spatial kernel defined in (12). In the following section, we describe the spatio-temporal density function that we use to estimate the sample observation times and locations. We also explain how we infer the model parameters given a set of samples.

### C. Predicting Sample Observations

To estimate the sample observation times and locations, we introduce a probabilistic model which represents the spatio-temporal sample observations. We estimate the observation time  $t_i$  and the location  $\mathbf{s}_i = (m_i, n_i)$  of the sample  $\mathbf{x}_i$  as the conditional mean of the random variables  $\tilde{t}_i$  and  $\tilde{\mathbf{s}}_i = (\tilde{m}_i, \tilde{n}_i)$  as

$$\hat{t}_i = \mathbb{E}[\tilde{t}_i | H(t_{i-1})] = \int_{t_{i-1}}^{\infty} t' f_{\tilde{t}_i}(t' | H(t_{i-1})) dt', \quad (18)$$

$$\hat{m}_i = \mathbb{E}[\tilde{m}_i | H(t_{i-1})] = \int_S m' f_{\tilde{\mathbf{s}}_i}(m' | H(t_{i-1})) ds, \quad (19)$$

$$\hat{n}_i = \mathbb{E}[\tilde{n}_i | H(t_{i-1})] = \int_S n' f_{\tilde{\mathbf{s}}_i}(n' | H(t_{i-1})) ds, \quad (20)$$

where the integration in (19) and (20) is over the spatial region  $S$ . In (18)-(20), we compute the density functions  $f_{\tilde{t}_i}$  and  $f_{\tilde{\mathbf{s}}_i}$  from the joint density function  $f_{\tilde{t}_i, \tilde{\mathbf{s}}_i}$  via marginalizing over space and time as

$$\begin{aligned} f_{\tilde{t}_i}(t) &= \int_S f_{\tilde{t}_i, \tilde{\mathbf{s}}_i}(t, \mathbf{s} | H(t_{i-1})) ds, \\ f_{\tilde{\mathbf{s}}_i}(\mathbf{s}) &= \int_{t_{i-1}}^{\infty} f_{\tilde{t}_i, \tilde{\mathbf{s}}_i}(t, \mathbf{s} | H(t_{i-1})) dt. \end{aligned} \quad (21)$$

We define the joint density function,  $f_{\tilde{t}_i, \tilde{\mathbf{s}}_i}$ , using the extended definition of the spatio-temporal intensity in (7) and the density function in (5). Hence, we define the joint density function as

$$\begin{aligned} f_{\tilde{t}_i, \tilde{\mathbf{s}}_i}(t, \mathbf{s} | H(t_{i-1})) &= \lambda(t, \mathbf{s} | H(t_{i-1})) e^{-\Lambda_{t_{i-1}}(t, \mathbf{s})}, \\ \Lambda_{t_{i-1}}(t, \mathbf{s}) &= \int_{t_{i-1}}^t \int_S \lambda(t', \mathbf{s}' | H(t_{i-1})) ds' dt'. \end{aligned} \quad (22)$$

Instead of using the conditional intensity definition in (10), we use a more compact and smoother expression as in (9) with subregion scores, which is the weighted combination of the intensity functions  $\lambda(t, \mathbf{s}|H(t_{i-1}))$  with the spatial subregion scores  $\mathbf{p}(\mathbf{s})$ . Therefore,

$$\lambda(t, \mathbf{s}|H(t_{i-1})) = \mathbf{p}(\mathbf{s})^T \boldsymbol{\lambda}(t, \mathbf{s}|H(t_{i-1})). \quad (23)$$

Note that in (18)-(22), the computations include integrations. We estimate them by a Riemann sum [26]. Thus, we uniformly sample points in space and time over the integration intervals. For example, the computation of the exponent  $\Lambda_{t_{i-1}}(t, \mathbf{s})$  of the joint density function  $f_{\tilde{t}_i, \tilde{\mathbf{s}}_i}$  is calculated as

$$\Lambda_{t_{i-1}}(t, \mathbf{s}) = \frac{1}{M} \sum_{t_j, \mathbf{s}_j} \lambda(t_j, \mathbf{s}_j|H(t_{i-1}))T|S|, \quad (24)$$

where  $M$  is the number of points used in the calculation. We observe in our simulations by selecting sufficiently large  $M$ , we observe no negative effects.  $t_j$  and  $\mathbf{s}_j$  are the times and locations of the sampled points,  $\mathbf{x}_j$ . Finally,  $T$  is the length of the temporal interval over which the integration is computed, i.e.  $T = t - t_{i-1}$  in (22) and  $S$  is the total spatial area over which the integration is computed, i.e.  $|S| = (n_u - n_l) \times (n_u - n_l)$ .

Note that the integration in (18) and (21) are over an infinitely long temporal interval. Therefore, it is not possible to directly apply the formulation in (24). However, by definition in (4), the conditional intensity is non-negative. Hence, the density function computed in (22) is a monotonically decreasing function of time. Thus, we simulate the integration in (21) up to a certain time. We observe in our experiments that selecting this time as  $20\Delta t$  is sufficient, where  $\Delta t$  is the mean inter-arrival time between samples, which is computed as  $\Delta t = (t_T - t_1)/I$ .

**Remark 4.** *It is possible to estimate the integrations via Monte Carlo Integration method [27]. Monte Carlo Integration is preferred over Riemann sum estimation when the integrated function has abrupt changes. However, we can readily increase the number of uniform samples  $M$  in (24) to overcome this problem depending on the application.*

#### D. Likelihood Optimization and Model Parameter Inference

In this subsection, we first group the adaptive decision tree and Hawkes process parameters. Then, we formulate an objective function and introduce our gradient based parameter optimization procedure.

A node,  $n_r$ , is parametrized by the weights  $\mathbf{w}_{n_r}$  and the threshold  $b_{n_r}$ . The decision tree parameters are the collection of node parameters. Therefore, the model parameters are  $\theta_{\text{tree}} = \{(\mathbf{w}_{n_r}, b_{n_r})\}_{r=1}^R$  for a decision tree with  $R$  nodes. Similarly, we can group the parameters in (23) by inspecting (11). For a subregion  $S_k$ , the conditional intensity is  $\lambda_k$  with parameters  $\mu_k$  and  $\gamma_k$ . Including the interaction matrix  $\Gamma$ , for  $K$  subregions Hawkes parameters are  $\theta_{\text{hawkes}} = \{\Gamma, \{(\mu_k, \gamma_k)\}_{k=1}^K\}$ .

We group the set of parameters,  $\theta_{\text{tree}}$  and  $\theta_{\text{hawkes}}$ , into a single set  $\Theta = [\theta_{\text{tree}}, \theta_{\text{hawkes}}]$ , which we call the

model parameters. Full notation for the conditional intensity  $\lambda(t_j, \mathbf{s}_j|H(t_j))$  and the density function  $f_{\tilde{t}_i, \tilde{\mathbf{s}}_i}(t, \mathbf{s}|H(t_i))$  should be  $\lambda(t_j, \mathbf{s}_j|H(t_i), \Theta)$  and  $f_{\tilde{t}_i, \tilde{\mathbf{s}}_i}(t, \mathbf{s}|H(t_i), \Theta)$  respectively. However, with an abuse of notation, we drop the parameters  $\Theta$ , for notational simplicity.

For a set of model parameters  $\Theta$ , we measure the fitness of our representation with the likelihood function

$$\mathcal{L}(X) = \prod_{i=1}^I f_{\tilde{t}_i, \tilde{\mathbf{s}}_i}(t_i, \mathbf{s}_i|H(t_{i-1})). \quad (25)$$

We aim to find a set of optimal parameters  $\Theta^*$ , which yields a likelihood  $\mathcal{L}(X|\Theta^*)$  that exceeds a certain tolerance level  $\mathcal{L}_{\text{tol}}$ , i.e.

$$\mathcal{L}(X|\Theta^*) \geq \mathcal{L}_{\text{tol}} \quad (26)$$

To this end, we split our data  $X$  into three groups; training ( $X_{\text{train}} = \{\mathbf{x}_i\}_{i=1}^{I_{\text{train}}}$ ), validation ( $X_{\text{val}} = \{\mathbf{x}_i\}_{i=I_{\text{train}}+1}^{I_{\text{val}}}$ ) and test ( $X_{\text{test}} = \{\mathbf{x}_i\}_{i=I_{\text{val}}+1}^I$ ). We search for an optimal parameter in the training set using (25) but measure the performance on the validation and test set using the metric defined in (2).

Since our aim is to maximize the likelihood in (25), we search the optimal parameters  $\Theta^*$  with the stochastic gradient-ascent algorithm [28]. To simplify the gradient expressions, we maximize the log-likelihood  $\tilde{\mathcal{L}} = \log \mathcal{L}$ , which is

$$\tilde{\mathcal{L}}(X|\Theta) = \sum_{i=1}^I \log f_{\tilde{t}_i, \tilde{\mathbf{s}}_i}(t_i, \mathbf{s}_i|H(t_{i-1})). \quad (27)$$

Substituting the density function  $f_{\tilde{t}_i, \tilde{\mathbf{s}}_i}(t_i, \mathbf{s}_i|H(t_{i-1}))$  in (27) with the formulation in (22), we obtain the expression

$$\tilde{\mathcal{L}}(X|\Theta) = \sum_{i=1}^I \log \lambda(t_i, \mathbf{s}_i|H(t_{i-1})) - \sum_{j=1}^J \Lambda_{t_{i-1}}(t_j, \mathbf{s}_j), \quad (28)$$

which consists of two terms,  $\mathcal{L}_p$  and  $\mathcal{L}_n$ .  $\mathcal{L}_n$ , can be accumulated and expressed as a single integral as

$$\mathcal{L}_n = \int_{t_0}^T \int_S \lambda(t', \mathbf{s}'|H(t_{i-1})) ds' dt', \quad (29)$$

where  $t_0$  is the simulation start time and  $T$  is the simulation end time. We simulate the integration in (29) using uniform sampling with  $J$  uniformly distant sample points between  $t_0$  and  $T$  as in [7]. Note that  $\mathcal{L}_p$  accumulates the log-intensities of the sample observations  $X = \{\mathbf{x}_i\}_{i=1}^N$  whereas  $\mathcal{L}_n$  accumulates the intensities of the rest of the spatio-temporal interval. We weight these terms as

$$\tilde{\mathcal{L}} = \mathcal{L}_p + \alpha \mathcal{L}_n, \quad (30)$$

to control the effect of both terms on  $\tilde{\mathcal{L}}$ .

Starting from a random set of model parameters,  $\Theta_0$ , we update this set with stochastic gradient updates. For a model parameter  $\theta_i \in \Theta_i$ , we have

$$\theta_{i+1} = \theta_i + \eta \nabla_{\theta} \tilde{\mathcal{L}}(X_B), \quad (31)$$

where  $X_B$  is a mini-batch with  $X_B \subset X$  and  $X_B = \{\mathbf{x}_b\}_{b=1}^B$ .  $\eta$  is the learning rate that scales the parameter updates and  $\nabla_{\theta} \tilde{\mathcal{L}}(X_b)$  is the derivative of  $\tilde{\mathcal{L}}(X_b)$  with respect to  $\theta$ . From

(28) and (30) we have,

$$\frac{\partial \tilde{\mathcal{L}}(X_b)}{\partial \theta} = \frac{1}{B} \sum_{b=1}^B \left( \left[ \frac{1}{\lambda_k(t_b, \mathbf{s}_b)} \right]_{k=1}^K + \alpha \mathbb{1}_K \right) \odot \frac{\partial \boldsymbol{\lambda}(t_b, \mathbf{s}_b)}{\partial \theta}. \quad (32)$$

Therefore, the partial derivatives of  $\boldsymbol{\lambda}$  with respect to the Hawkes parameters are given as,

$$\frac{\partial \lambda_k(t_b, \mathbf{s}_b)}{\partial \mu_k} = p_k(\mathbf{s}_b), \quad (33)$$

$$\frac{\partial \lambda_k(t_b, \mathbf{s}_b)}{\partial \boldsymbol{\Gamma}_{i,k}} = \sum_{\mathbf{x} \in X_H(t_b)} p_i(\mathbf{s}) e^{\gamma_k(t-t_b)} \quad (34)$$

and

$$\frac{\partial \lambda_k(t_b, \mathbf{s}_b)}{\partial \gamma_k} = \boldsymbol{\Gamma}_{:,k}^T \sum_{\mathbf{x} \in X_H(t_b)} \mathbf{p}_k(\mathbf{s})(t-t_b) e^{\gamma_k(t-t_b)}. \quad (35)$$

Similarly we compute the derivatives for the tree parameters and latent variables as,

$$\frac{\partial \boldsymbol{\lambda}(t_b, \mathbf{s}_b)}{\partial \mathbf{p}} = \boldsymbol{\lambda}(t_b, \mathbf{s}_b) \odot (\mathbb{1}_K + \mathbf{J}^T \mathbf{p}(\mathbf{s}_b)), \quad (36)$$

where  $\mathbf{J}$  is the jacobian matrix with elements  $\mathbf{J}_{i,j} = \partial \lambda_i / \partial p_j$ . For the threshold  $b_{n_r}$  we have

$$\frac{\partial \mathbf{p}(\mathbf{s}_b)}{\partial b_{n_r}} = \sum_{k=1}^K \prod_{\substack{l=1, \\ l \neq l'}}^L \pi(\mathbf{x}_b, v_k^{(l)}, \tau_k^{(l)}) \sigma(1-\sigma), \quad (37)$$

where  $l'$  is the level of the node  $n_r$  and  $\sigma = \sigma(\mathbf{w}_{n_r}^T \mathbf{s}_b + b_{n_r})$ . Similarly, we have

$$\frac{\partial \mathbf{p}(\mathbf{s}_b)}{\partial \mathbf{w}_{n_r}} = \sum_{k=1}^K \prod_{\substack{l=1, \\ l \neq l'}}^L \pi(\mathbf{x}_b, v_k^{(l)}, \tau_k^{(l)}) \sigma(1-\sigma) \mathbf{s}_b. \quad (38)$$

Note that the intensity  $\lambda(t, \mathbf{s} | H(t))$  defined in (7) should be non-negative by definition. However, we optimize the model parameters with gradient updates. Therefore, we use softplus function as

$$\tilde{\lambda}(t, \mathbf{s} | H(t)) = \log(1 + e^{\lambda(t, \mathbf{s} | H(t))}) \quad (39)$$

to make sure it is non-negative through all iterations.

We define the set  $\rho$ , which contains all parameters that are not included in the model parameters set. We call this set the hyperparameters and it includes the parameters:  $L$ , the decision tree depth;  $J$ , the number of samples for integration simulations in (18), (29);  $\phi$ , the number of past samples in the intensity computation in (4);  $\eta$ , the learning rate that scales the parameter updates;  $\mathcal{L}_{\text{tol}}$ , the tolerance level for the log-likelihood;  $\alpha$ , the log-likelihood weighting parameter.

We present the iterative optimization procedure in Algorithm 1 as a pseudocode. In Algorithm 1, we initialize a depth- $L$  decision tree with random parameters and a Hawkes model for  $K = 2^L$  spatial subregions with random parameters as well. At iteration step  $i$ , we compute the parameter updates,  $\Delta \Theta_i$ .  $\Delta \Theta_i$  is the vector of derivatives of the log-likelihood function  $\tilde{\mathcal{L}}$  with respect to the model parameters. Then, we

---

**Algorithm 1** Gradient based training procedure.

---

**Require:** Hyperparameters:  $\rho$

```

 $i = 0$ 
Randomly initialize depth- $L$  tree,  $\theta_{\text{tree}}$ .
Randomly initialize Hawkes parameters  $\theta_{\text{hawkes}}$ .
 $\Theta_i = [\theta_{\text{tree}}, \theta_{\text{hawkes}}]$ 
 $\tilde{\mathcal{L}}_i \leftarrow \log \mathcal{L}(X | \Theta_i)$ 
while  $\tilde{\mathcal{L}}_i < \log \mathcal{L}_{\text{tol}}$  do
  Compute  $\mathcal{L}_p$  in (30)
  Compute  $\mathcal{L}_n$  in (30)
  Compute updates,  $\Delta \Theta_i$ 
   $\Theta_{i+1} \leftarrow \Theta_i + \eta * \Delta \Theta_i$ 
   $i \leftarrow i + 1$ 
end while
Compute performance,  $L(\hat{X}_{\text{val}}, X_{\text{val}})$  as in (2)

```

---

compute the log-likelihood with the updated model parameters and check whether it exceeds the tolerance level,  $\mathcal{L}_{\text{tol}}$ . Once exceeded, we compute the MSE score on the validation set.

We perform several sessions of training on the same training set with different hyperparameters. We tune the hyperparameters on the validation set by comparing the MSE scores after the training is over. Once we find the best set of hyperparameters, we compute the MSE score on the test set for once and report it.

In Algorithm 1, the training algorithm uses the whole training set for parameter optimization. Therefore, we also introduce an online training procedure in which we update the model parameters as we observe new samples.

Note that the objective function in (27) require all past sample observations and uniformly sampled points from time  $t_0$  to  $T$ . Thus, it is not suitable for online setup since the sequence of past samples will expand as new samples are observed. To this end, we modify the objective function for online setup. Suppose that the sample  $\mathbf{x}_i = [t_i, \mathbf{s}_i]$  is observed. We compute the term  $\mathcal{L}_p$  as

$$\mathcal{L}_{p_{\text{online}}} = \log \lambda(t_i, \mathbf{s}_i | H(t_{i-1})). \quad (40)$$

Similarly, we modify the term  $\mathcal{L}_n$  as

$$\mathcal{L}_{n_{\text{online}}} = - \sum_{j=1}^J \lambda(t_j, \mathbf{s}_j | H(t_{i-1})) \quad (41)$$

in which we sample random points only in the interval  $[t_{i-1}, t_{i-1} + \delta_{i-1}]$  where  $\delta_{i-1}$  is the length of the temporal interval, i.e.  $t_j \in [t_{i-1}, t_{i-1} + \delta_{i-1}]$ . We observe in our experiments that setting  $\delta_{i-1}$  to  $20\Delta t$  is sufficient. As a result, we train our model in online setup as the updates will only depend on the most recent sample observations. This procedure is given in Algorithm 2.

In Algorithm 2, we append the newly arrived sample,  $\mathbf{x}$  to the set  $X$ . However, we only keep the  $\phi$  most recent samples in that set as the rest of the samples do not effect the intensity computations. Therefore, with Algorithm 2, we present a setup that can infer the model parameters under nonstationary source as it updates the model parameters with the newly observed samples.

**Algorithm 2** Online training procedure.

---

**Require:** Hyperparameters:  $\rho$   
 Randomly initialize depth- $L$  tree,  $\theta_{\text{tree}}$ .  
 Randomly initialize Hawkes parameters  $\theta_{\text{hawkes}}$ .  
 Initialize  $X = \{\}$   
 $\Theta \leftarrow [\theta_{\text{tree}}, \theta_{\text{hawkes}}]$   
**while**  $\mathbf{x}$  arrives **do**  
 $X \leftarrow \{X_{\phi-1}, \mathbf{x}\}$   
 Compute  $\mathcal{L}_{\text{ponline}}, \mathcal{L}_{\text{nonline}}$  in (40), (41)  
 Compute updates,  $\Delta\Theta$   
 $\Theta \leftarrow \Theta + \eta * \Delta\Theta$   
**end while**

---

Models	L	$\phi$	$\alpha$	N
Exp-1	2	20	1000	5000
Exp-2	4	20	1000	5000
TreeHawkes	5	20	2000	5000

**TABLE I:** Hyperparameters selected in the experiments.

**Remark 5.** In both Algorithm 1 and 2, we randomly initialize a set of model parameters and update them with the gradient ascent method in (31). However, for faster parameter convergence in Algorithm 1 and 2, we also optimize the model parameters with the ADAM optimizer [29]. The ADAM optimizer requires only the first order gradients. Thus, it does not bring any additional computational cost.

## IV. SIMULATIONS AND EXPERIMENTS

In this section, we explain the experimental setups and the performance of the model under these experiments. We also compare the performance of our model with baseline models. We split the experiments under two groups. In the first group, we simulate a sequence of spatio-temporal data using our model with arbitrary parameters. In the second group, we test the model on a real-life data to understand the inner working process of our algorithm.

For simplicity, instead of reporting two different error components for the spatial location estimations as in (1), we combine the errors in two spatial axes as

$$l(\hat{\mathbf{x}}_i, \mathbf{x}_i) = [(\hat{t}_i - t_i)^2, ((\hat{m}_i - m_i)^2 + (\hat{n}_i - n_i)^2)]$$

and report the MSE on the test set. Finally, we refer to the mean squared error in the temporal estimations as  $t - MSE$  and the mean squared error in the location estimations as  $s - MSE$ . We refer to our model as TreeHawkes in the figures and tables in this section.

## A. Experiments on Simulation Data

In this set of experiments, we create a simulated spatio-temporal sequence  $X$ , which is simulated by a TreeHawkes model. The model parameters are selected arbitrarily. We then generate the samples using the thinning algorithm [30]. We have performed two experiments on simulation data.

In both experiments, which we refer to as "Exp-1" and "Exp-2" in tables and figures, we construct a model with the hyperparameters shown in Table I. We then set the model

Models	t-MSE	s-MSE
Exp-1	0.072	9.34
Exp-2	0.081	8.71
TreeHawkes	0.178	5.78
CNN	0.264	25.47
Linear	0.271	33.28

**TABLE II:** Test error scores achieved on simulated data and by TreeHawkes, and the baseline models on real-life data.

parameters arbitrarily. We generate 5000 samples in the interval starting from the time  $t_0 = 0$  and ending at  $T = t_{5000}$ . We then construct a model with the same architecture and the same hyperparameters, but initialize with random model parameters. Using the procedure described in Algorithm 1, we then fit the model on the simulated data. The whole sequence,  $X = \{\mathbf{x}_i\}_{i=1}^{5000}$ , is divided into training, validation and test sets with lengths 3000, 1000 and 1000 respectively. Moreover, we confine the spatial region that the samples can be observed to the region  $S = \{(m, n) \in \mathbb{R}^2 \mid -10 < m < 10, -10 < n < 10\}$ . At the end of every epoch, we record the  $t - MSE$  and  $s - MSE$  on the validation set. These errors can be seen in Fig. 3. Test score for both experiments are shown in Table II.

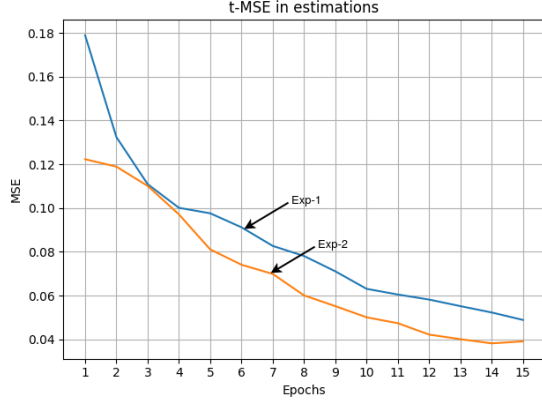
## B. Experiments on Real-life Data

In this set, we perform experiments on a real life spatio-temporal data. We have selected the Significant Earthquakes Dataset for the experimentation [31]. This dataset is provided by the National Earthquake Information Center (NEIC) and it includes the date, time, location, depth, magnitude, and source records of every earthquake occurred worldwide from 1900 to 2020. Predicting the times and the locations of earthquakes fits our problem description as we can model the earthquake events as the spatio-temporal samples.

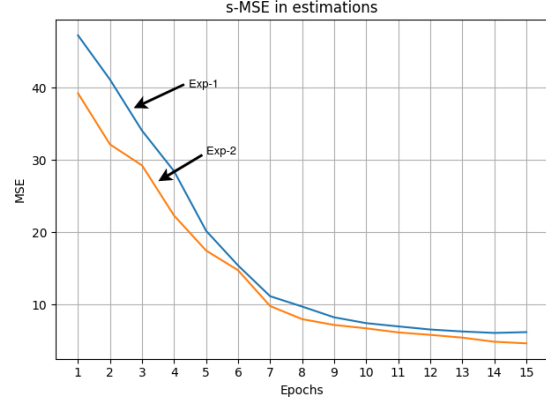
The dataset contains only significant earthquakes with magnitudes higher than 5.5, hence it does not include aftershocks, which could be modeled effectively by the self-exciting formulation of the Hawkes intensity. Therefore, we test our model in a spatial region where the earthquakes occur frequently. To this end, we select the spatial region  $S$  between the latitudes  $32.00^\circ$  and  $72.00^\circ$  and between the longitudes  $110.0^\circ$  and  $180.0^\circ$ . This region covers Japan, Korea and the east of China and Russia.

We extract a spatio-temporal sequence  $X = \{\mathbf{x}_i\}_{i=1}^N$  from the dataset, which has the samples  $\mathbf{x}_i = [t_i, \mathbf{s}_i]$ .  $\{t_i\}_{i=1}^N$  are the times at which the earthquakes have occurred. In the dataset, earthquake times were recorded as dates. We convert these dates relative to the time of the first earthquake record in seconds. We then convert the seconds to months by scaling, i.e.  $\{t_i / (3600 \times 24 \times 30)\}_{i=1}^N$ . Spatial locations of the earthquakes are recorded in latitudes and longitudes. We have scaled these latitude and longitude values to fit the spatial region  $S = \{(m, n) \in \mathbb{R}^2 \mid -10 < m < 10, -10 < n < 10\}$  centered around the middle point of the region, i.e.  $52.00^\circ, 145.00^\circ$ .

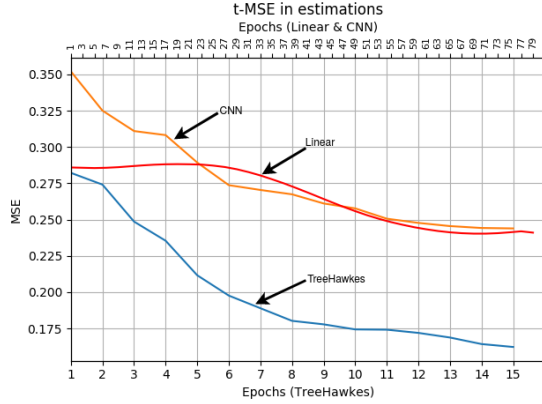
We train our model with the procedure described in Algorithm 1 with the hyperparameters shown in Table I. We report the  $t - MSE$  and  $s - MSE$  on validation set as in Fig. 3. Finally, we report the errors in the test set in Table II.



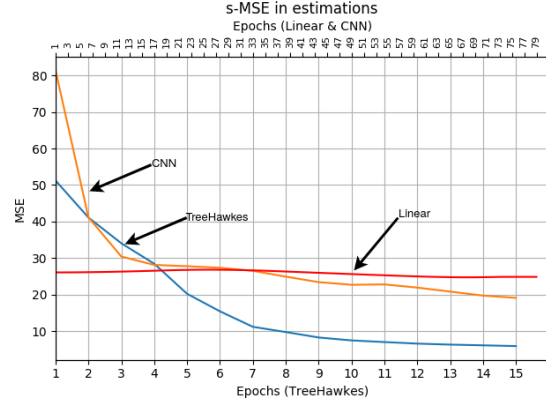
(a) MSE in sample observation times for simulation data experiments. Exp-1 refers to the experiment with 2-level decision tree whereas the Exp-2 refers to the experiment with 3-level decision tree.



(b) MSE in sample observation locations for simulation data experiments. Exp-1 refers to the experiment with 2-level decision tree whereas the Exp-2 refers to the experiment with 3-level decision tree.



(c) MSE in sample observation times for the introduced model.



(d) MSE in sample observation locations for the introduced model.

**Fig. 3:** Validation MSE scores obtained at the end of each iteration described in Algorithm 1 for both the simulated data and the real-life earthquake dataset. Performance of the introduced model is also compared with a baseline model in figures (c) and (d). We refer to our model as "TreeHawkes" and to the baseline models as "Linear" and "CNN".

To compare our model, we train a linear regression model, which predicts the time and space difference between the last earthquake event and the next earthquake event. This model uses the most recent 40 time and space differences between the events to predict the next one. Validation errors for this model are shown in Fig. 3, which is labeled as "Linear". Finally, we report the test error score in Table II.

We perform a similar experiment on a Convolutional Neural Network (CNN) model, which operates on a spatio-temporal window. To test the model on the dataset, we first discretize the data by constructing a 3-dimensional frame with shape  $(T, M, N)$  where  $T$  is the number of temporal bins and it corresponds to the constant length time intervals starting from the time of the first earthquake record and ends at the time of the last one. We select the number of temporal bins  $T$  so that a bin corresponds to 5 days. Similarly, we discretize the spatial axes into  $M$  and  $N$  bins. We select the number of spatial bins as  $M, N = (30, 30)$ . We then place the spatio-temporal samples,  $\mathbf{x}_i$  into the spatial and temporal bins that they fall into. Thus, if an earthquake has occurred in the spatio-temporal interval of a bin, that bin is labeled as 1, otherwise 0. The

spatial frames in the discretized data are indexed with time, i.e.  $\{Y^{(i)}\}_{i=1}^T$ . Each frame,  $Y^{(t)}$ , is a 2-dimensional spatial frame with size  $(M, N)$ .

The CNN model is a three-layer model and the last layer is a normalization layer. We iteratively make predictions for every spatial frame at each time step. At step  $t$ , the model takes the most recent 20 spatio-temporal frames, i.e.  $\{Y^{(i)}\}_{i=t-19}^t$  as input and applies  $30 \times 3 \times 3$  convolutional kernels with zero padding at the first two layers. The output of the first two layers is therefore  $30 \times M \times N$  frames. The last layer normalizes the output scores over all elements with min-max scaling to the interval  $[0, 1]$ . We estimate the time and location of an earthquake by computing the mean of the model scores of 30 output frames for three axes.

The CNN model generates 30 output frames at a time. We compute the mean squared distance between the 30 output frames and the 30 ground truth frames. We then update the parameters of the CNN model with the ADAM optimizer minimizing the mean squared error in the 30 output frames over the whole training sequence.

Finally, we compute the MSE score of the CNN model by

averaging the squared errors between the ground truth samples and the estimated earthquake events that are temporally closest but predicted earlier than the ground truth samples. Hence, for a ground truth sample,  $\mathbf{x}_i = [t_i, \mathbf{s}_i]$ , we match the prediction  $\hat{\mathbf{x}} = [\hat{t}, \hat{\mathbf{s}}]$  that is the temporally closest, i.e.  $\hat{t} = \arg \min_t (t_i - \hat{t})^2$ , and earlier than the ground truth sample, i.e.  $\hat{t} \leq t_i$ . Under this setup, we report the validation performance in Fig. 3. Finally, we report the errors in the test set in Table II.

Fig. 3 shows that our model outperforms both the Linear and the CNN model. The Linear model assumes an autoregressive relation between the past temporal and spatial differences without any nonlinearity. Moreover, temporal and spatial locations of the samples have additive effects on each other, which degrades the performance as shown in Fig. 3. Due to the simple structure of the model, the error on the validation set converges to a level, which is considerably higher than the level achieved by our algorithm. Although the CNN model is a nonlinear autoregressive model, its performance is limited by the sparsity and the nonstationarity of the earthquake data. Similar to the errors in temporal predictions, both the Linear and CNN models converge to a certain level. This is due to the linear and additive autoregressive relations in the spatial predictions. On the other hand, our model shows superior performance in both the temporal and spatial predictions. This is due to the nonlinear modeling of the sample observation times and locations with point processes in adaptive subregions.

## V. CONCLUDING REMARKS

In this paper, we introduce a point process that can model spatio-temporal sequences of samples. Our approach is based on the Hawkes process formulation, which has a self-exciting mechanism. We extend the formulation of the Hawkes process to add spatial connections between the samples. We also partition the spatial region into adaptive subregions and model the sequence of samples in each spatial subregion with different parameters. Therefore, our model is able to capture patterns in space and time for nonstationary data. We introduce a likelihood based objective function, which jointly optimizes the model parameters. Finally, we show that our approach can be applied to online setup with simple stochastic gradient updates of the model parameters. We provide experimental results that compare our approach to baseline models on a real-life dataset, which demonstrate the significant performance gains due to the adaptiveness to regions and joint optimization of spatial regions and Hawkes process parameters.

## REFERENCES

- [1] H. Kanamori, "Earthquake prediction: An overview," 2003.
- [2] V. Roberto and C. Chiaruttini, "Seismic signal understanding: a knowledge-based recognition system," *IEEE Transactions on Signal Processing*, vol. 40, no. 7, pp. 1787–1806, 1992.
- [3] Z. Gao, X. Wang, Y. Yang, C. Mu, Q. Cai, W. Dang, and S. Zuo, "Eeg-based spatio-temporal convolutional neural network for driver fatigue evaluation," *IEEE Transactions on Neural Networks and Learning Systems*, vol. 30, no. 9, pp. 2755–2763, 2019.
- [4] C. Jiang, Y. Chen, and K. R. Liu, "Evolutionary dynamics of information diffusion over social networks," *IEEE Transactions on Signal Processing*, vol. 62, no. 17, pp. 4573–4586, 2014.
- [5] P. Zhang, I. Nevat, G. W. Peters, G. Xiao, and H.-P. Tan, "Event detection in wireless sensor networks in random spatial sensors deployments," *IEEE Transactions on Signal Processing*, vol. 63, no. 22, pp. 6122–6135, 2015.
- [6] B. Wang, D. Zhang, D. Zhang, P. J. Brantingham, and A. L. Bertozzi, "Deep learning for real time crime forecasting," *arXiv preprint arXiv:1707.03340*, 2017.
- [7] H. Mei and J. M. Eisner, "The neural hawkes process: A neurally self-modulating multivariate point process," in *Advances in Neural Information Processing Systems*, 2017, pp. 6754–6764.
- [8] J. L. Elman, "Finding structure in time," *Cognitive Science*, vol. 14, no. 2, pp. 179–211, 1990.
- [9] M. Han, J. Xi, S. Xu, and F.-L. Yin, "Prediction of chaotic time series based on the recurrent predictor neural network," *IEEE Transactions on Signal Processing*, vol. 52, no. 12, pp. 3409–3416, 2004.
- [10] J. Baltersee and J. A. Chambers, "Nonlinear adaptive prediction of speech with a pipelined recurrent neural network," *IEEE Transactions on Signal Processing*, vol. 46, no. 8, pp. 2207–2216, 1998.
- [11] S. Hochreiter and J. Schmidhuber, "Long short-term memory," *Neural Computation*, vol. 9, no. 8, pp. 1735–1780, 1997.
- [12] Y. LeCun, Y. Bengio, and G. Hinton, "Deep learning," *Nature*, vol. 521, no. 7553, pp. 436–444, 2015.
- [13] L. Duan, T. Hu, E. Cheng, J. Zhu, and C. Gao, "Deep convolutional neural networks for spatiotemporal crime prediction," in *Proceedings of the International Conference on Information and Knowledge Engineering (IKE)*. The Steering Committee of The World Congress in Computer Science, Computer ..., 2017, pp. 61–67.
- [14] B. Wang, P. Yin, A. L. Bertozzi, P. J. Brantingham, S. J. Osher, and J. Xin, "Deep learning for real-time crime forecasting and ternarization," *Chinese Annals of Mathematics, Series B*, vol. 40, no. 6, pp. 949–966, 2019.
- [15] R. W. Heath, M. Kountouris, and T. Bai, "Modeling heterogeneous network interference using poisson point processes," *IEEE Transactions on Signal Processing*, vol. 61, no. 16, pp. 4114–4126, 2013.
- [16] G. O. Mohler, M. B. Short, P. J. Brantingham, F. P. Schoenberg, and G. E. Tita, "Self-exciting point process modeling of crime," *Journal of the American Statistical Association*, vol. 106, no. 493, pp. 100–108, 2011.
- [17] N. Du, H. Dai, R. Trivedi, U. Upadhyay, M. Gomez-Rodriguez, and L. Song, "Recurrent marked temporal point processes: Embedding event history to vector," in *Proceedings of the 22nd ACM SIGKDD International Conference on Knowledge Discovery and Data Mining*, 2016, pp. 1555–1564.
- [18] D. J. Daley and D. Vere-Jones, *An introduction to the theory of point processes: volume II: general theory and structure*. Springer Science & Business Media, 2007.
- [19] A. Krizhevsky, I. Sutskever, and G. E. Hinton, "Imagenet classification with deep convolutional neural networks," in *Advances in Neural Information Processing Systems*, 2012, pp. 1097–1105.
- [20] R. Socher, Y. Bengio, and C. D. Manning, "Deep learning for nlp (without magic)," in *Tutorial Abstracts of ACL 2012*. Association for Computational Linguistics, 2012, pp. 5–5.
- [21] B. Wang, X. Luo, F. Zhang, B. Yuan, A. L. Bertozzi, and P. J. Brantingham, "Graph-based deep modeling and real time forecasting of sparse spatio-temporal data," *arXiv preprint arXiv:1804.00684*, 2018.
- [22] E. Lewis and G. Mohler, "A nonparametric em algorithm for multiscale hawkes processes," *Journal of Nonparametric Statistics*, vol. 1, no. 1, pp. 1–20, 2011.
- [23] T. K. Ho, "Random decision forests," in *Proceedings of 3rd international conference on document analysis and recognition*, vol. 1. IEEE, 1995, pp. 278–282.
- [24] J. Ali, R. Khan, N. Ahmad, and I. Maqsood, "Random forests and decision trees," *International Journal of Computer Science Issues (IJCSI)*, vol. 9, no. 5, p. 272, 2012.
- [25] F. M. Willems, Y. M. Shtarkov, and T. J. Tjalkens, "The context-tree weighting method: basic properties," *IEEE Transactions on Information Theory*, vol. 41, no. 3, pp. 653–664, 1995.
- [26] B. P. Flannery, W. H. Press, S. A. Teukolsky, and W. Vetterling, "Numerical recipes in c," *Press Syndicate of the University of Cambridge, New York*, vol. 24, p. 78, 1992.
- [27] R. E. Caflisch, "Monte carlo and quasi-monte carlo methods," *Acta Numerica*, vol. 7, pp. 1–49, 1998.
- [28] L. Bottou, "Large-scale machine learning with stochastic gradient descent," in *Proceedings of COMPSTAT'2010*. Springer, 2010, pp. 177–186.
- [29] D. P. Kingma and J. Ba, "Adam: A method for stochastic optimization," *arXiv preprint arXiv:1412.6980*, 2014.
- [30] Y. Ogata, "On lewis' simulation method for point processes," *IEEE Transactions on Information Theory*, vol. 27, no. 1, pp. 23–31, 1981.
- [31] N. E. I. Center, "Significant earthquakes," <https://www.usgs.gov/natural-hazards/earthquake-hazards/earthquakes>, 2020.